Available online at www.sciencedirect.com
SCIENCE DIRECT®

Journal of the European Ceramic Society 24 (2004) 705–715

www.elsevier.com/locate/jeurceramsoc

# Proton—conducting ceramics as electrode/electrolyte—materials for SOFCs: Preparation, mechanical and thermal-mechanical properties of thermal sprayed coatings, material combination and stacks

G. Fehringer, S. Janes*, M. Wildersohn, R. Clasen

*Department of Powder Technology, Saarland University, Building 43, D-66041 Saarbrücken, Germany*

Received 28 June 2002; received in revised form 20 March 2003; accepted 6 April 2003

**Abstract**

This part of investigation includes the synthesis, preparation and examination of the cathode lanthan–strontium–manganite (ULSM) as bulk material, the BCN electrolyte as coating and the cermet anode (BCN/Ni) as coating too. The ULSM powder was made by the conventional solid reaction of carbonates and oxide. The ULSM samples were cold pressed and sintered at temperatures between 1400 and 1600 °C. The measurement of the mechanical properties like bending strength (room and high temperature), Young modulus ($E$), modulus of rigidity ($G$), Poison's ratio, hardness and fracture toughness were done for the ULSM bulk material. The highest values of bending strength, $E$ and $G$ was found to be 85 MPa, 192 GPa and 46 GPa, respectively for the dense material and only 26 MPa bending strength for the porous material (30% pores). The hot bending strength (800 °C) was also in the range of 25 MPa for the porous material. In the case of BCN coatings cold bending strength was determined to 55 MPa for the dense material (99% TD). $E$- and $G$-moduli were in the range of 190 and 46 GPa in maximum while Poisońs ratio was about 0.35. Vickers hardness was resulted in a maximum value of 5 GPa while Poison's ratio was about 0.35. Finally the cold bending strength of the porous cermet coatings (30% porosity) was measured to 54 MPa with an $E$-modulus of 15 GPa. The Vickers hardness was about 0.2 GPa and the coefficient of thermal expansion about $11\times10^{-6}$ $K^{-1}$. Finally, the material combination cathode/electrolyte (ULSM–BCN) and the stacks (ULSM–BCN–BCN/Ni) were prepared and examined. The ULSM samples were cold pressed and sintered at temperature of 1400 °C with a porosity of about 30%. On the surface of ULSM the BCN electrolyte was prepared by plasma spraying. On the surface of the electrolyte the BCN/Ni anode was prepared by flame spraying. The measurement of the mechanical properties like bending strength (room and high temperature), Young modulus ($E$), adhesion strength were done for the material combination and adhesion strength and thermal shock resistance was measured for the stacks too. The values of bending strength and $E$ were found to 35 MPa and 62 GPa, respectively for the material combination. The hot bending strength (800 °C) was in the range of 59 MPa and an $E$ of 51 GPa. The adhesion strength was determined to 0.24 MPa for the material combination and 0.42 MPa for the stacks and the thermal shock resistance of the stacks was greater than 20 cycles.


*Keywords:* Fuel cells; (La,Sr)$MnO_3$; Manganites; Mechanical properties; Niobates; Niobate-cermet; Plasma spraying

## 1. Introduction

As exactly described in part I[1] proton conducting ceramics for a high-temperature solid oxide fuel cell (SOFC) barium–calcium–niobate (BCN) is a convenient material for the solid proton conducting electrolyte, lanthan–strontium–manganite (ULSM) is a convenient material for the cathode[2–7] and a cermet of BCN and nickel (50:50 vol.%) is the convenient material for the anode.[8,9]

The synthesis of the powder, the characterisation of the material phases, the preparation of the test samples and the mechanical and thermal properties of BCN18 and BCN18/Ni bulk material have been done.[1] In the case of La,Sr manganite[10] the mechanical and thermal properties of the bulk material must be tested also.

At the later application the thickness of the electrolyte and the anode material must be very small.[5] So coatings

* Corresponding author.
*E-mail address:* s.janes@matsci.uni-sb.de (S. Janes).

0955-2219/03/$ - see front matter © 2003 Elsevier Ltd. All rights reserved.
doi:10.1016/S0955-2219(03)00262-0

of these materials can be the solution. Coating techniques for ceramic materials are mainly thermal spraying methods, i.e. flame or plasma spraying. Therefore we investigate to prepare coatings by thermal spraying techniques.

Our concept to fabricate stacks afterwards of these fuel cell materials candidates is to prepare first the cathode by cold pressing and sintering techniques as substrate material. On this substrate BCN coating will be prepared by plasma spraying and final the cermet coating will be prepared by thermal spaying methods also on the surface of the BCN coating (Fig. 1). By this procedure the problems of joining can be minimised.

## 2. Synthesis of ULSM powder

The ULSM powder was synthesised by solid chemical reaction. Therefore the basic substances like calcium oxide, manganese oxide and strontium carbonate were mixed in a ball mill. Than the mixture was thermally treated in an electrical heated furnace. The calcination step was 1100 °C for 10 h.[3,4,7] The synthesised product was milled again and sieved, so that the powder had a grain size in the range of 1–10 μm. The powder was identified by X-ray diffraction as seen in Fig. 2. The diagram shows that the main peaks are identically with those of the JCPDS 40-1100 file, so that the resulted powder is really ULSM.

## 3. Preparation of ULSM test samples

The synthesised powder was uniaxial cold pressed in steel moulds to green bodies of $10\times10\times50$ mm$^3$. The pressure for the pressing was in the range of 40–80 MPa. The density of the pressed green bodies was in the range of 46–52% of the value for the theoretical density. For the mechanical measurements like three-point bending test, the green bodies were sintered as a function of sintering temperature in the range of 1400–1600 °C. The stopping time was between 1 and 4 h. The porosity of the sintered samples was 30% (sintering temperature 1400 °C) and 2% (sintering temperature 1600 °C). The porosity of 30% of the cathode material is necessary because of the desired permeability of gases. Afterwards the sintered parts were sawn in samples of $30\times4\times3$ mm$^3$ and polished. For four-point bending test the samples have had a dimension of $40\times4\times3$ mm$^3$ and were prepared in the same way as described earlier.

## 4. Mechanical and thermal properties of ULSM bulk material

The mechanical properties were examined due to bending strength at room temperature and higher temperatures, Young's modulus ($E$), modulus of rigidity ($G$), Poison's ratio, fracture toughness and hardness by Vickers.

The results of the three-point bending test at room temperature for the ULSM bulk material was concluded in the following Table 1. The table shows the bending strength as a function of density and porosity, respectively. The greatest value of 85 MPa maximum bending strength was achieved by the dense material (porosity 2%), while the lowest value of 12 MPa naturally was measured by the porous material (porosity 40%). We decided to the samples with a porosity of 30% because of its better handling and with a bending strength of 26 MPa.

The four-point bending tests were performed at a temperature of 800 °C and resulted in values of 25 MPa in maximum.

The moduli were calculated by the ultrasonic method on sintered stacks where the pulse timing of ultrasonic through the samples was measured. The results are

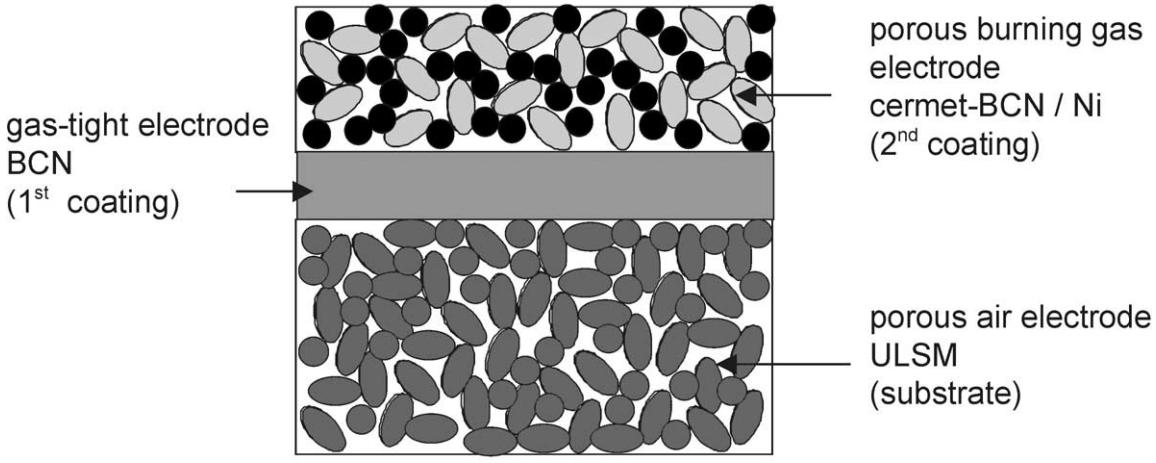


Fig. 1. Concept of preparation a proton conducting high temperature SOFC.

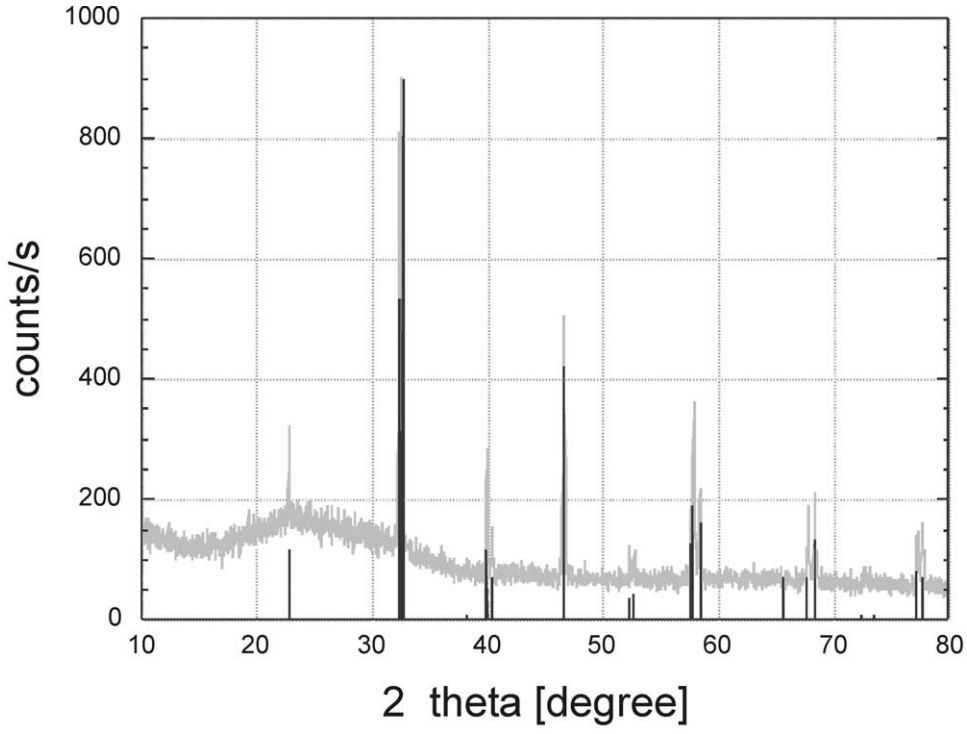


Fig. 2. X-ray diffraction pattern of ULSM.

Table 1
Bending strength and density of ULSM material

| Material | Bending-strength [MPa] | | Density [% TD] |
|---|---|---|---|
| | Min. | Max. | |
| ULSM | 40 | 85 | 98 |
| | 38 | 58 | 91 |
| | 15 | 19 | 85 |
| | 15 | 26 | 70 |
| | 10 | 12 | 60 |
| at 800 °C | 25 | | 76 |

Table 2
Physical properties of ULSM material

| | ULSM-bulk |
|---|---|
| Density [g/cm$^3$] | 6.1 (98% TD)[a] |
| Ultimate bending strength (cold) [MPa] | 40–85; 10 at 60% TD |
| Ultimate bending strength (800 °C) [MPa] | 25 |
| Hardness HV 1/10 [GPa] | 700 |
| $K_{IC}$ [MPa·m$^{0.5}$] | 0.8 |
| Modulus of elasticity [GPa] | 124 |
| Modulus of rigidity [GPa] | 46 |
| Poissons's ratio $\mu$ | 0.36 |
| Thermal shock resistance | 20 cycles |
| Thermal expansion coefficient $\alpha$ [K$^{-1}$] | $12.8\times10^{-6}$ K$^{-1}$ |

[a] Value of the theoretical density.

reported in Table 2. In the case of elastic modulus ($E$) and modulus of rigidity ($G$) the greatest values are in the order of 192, 46 GPa, respectively and a Poison's ratio of 0.36 (Table 2).

The results of the Vickers hardness combined with fracture toughness $K_{IC}$ are listed in Table 2, too. The resulted values were 0.7 GPa and 0.8 MPa·m$^{-0.5}$, while the thermal expansion coefficient was in the range of $12.4–12.8\times10^{-6}$K$^{-1}$ between ambient temperature and 1000 °C.

## 5. Preparation of plasma sprayed BCN coatings

Because of the necessary small thickness, dense and gas-tight of the solid BCN electrolyte plasma spraying technique was investigated. The plasma device mainly consists of a power supply with amplifier (METCO, 7MR-50), a control unit (METCO, 7M), a plasma gun (METCO, 9MB) and a powder feed unit (METCO, 4MP). The BCN powder with a grain size in the range of 20–45 μm was feed into the plasma flame consisting of a gas mixture of nitrogen and hydrogen (95:5). The plasma flame melted the powder grains so that melted droplets were catapult of the substrate surface. The high velocity of the droplets was caused by the high velocity of the plasma gases. After cooling the "droplets" adhered on the substrate surface and built up a coating.

First it was necessary to determine the spraying parameter by variation of, i.e. the quantity of the primary (nitrogen), secondary (95/5 nitrogen/hydrogen) and feeder gases (nitrogen), voltage, current, spraying distance from plasma gun to substrate and spraying time. The results of the investigation are listed in Table 3. The rich

Table 3
Optimisation of the plasma spraying parameters for BCN coatings

| Primary gas $N_2$ [l/min] | Secondary gas 95/5 $N_2H_2$ [l/min] | Feeder gas $N_2$ [l/min] | Power [kW] | Spraying distance [cm] | Spraying time [min] |
|---|---|---|---|---|---|
| Constant | **15** | 50 | 14 | **17** | 2 |
| **100** | 20 | **60** | 20 | 10 | 3 |
| | 25 | | **30** | | **5** |
| | | | 40 | | 10 |
| | | | 45 | | |

Substrate: alumina membrane.

marked values represented the optimum spraying parameters in regard to coatings with high densities. The values of the coating density were in the range of 97–99% TD (TD = value of the theoretical density). These experiments have been done by plasma spraying coatings on porous ceramic substrates with known densities. The purchasable substrates were membranes of alumina with a thickness of 2 mm.

The sprayed coatings were identified first by X-ray diffraction as seen in Fig. 3. The diagram also shows that the diffraction pattern is identically with those of the started BCN powder and the bulk material (JCPDS 50-0075 file).

For the determination of the mechanical properties the coatings were prepared by plasma spraying on steel substrates. Because of the great differences in the coefficient of thermal expansion between BCN and steel, no adhesion of coating and substrate can be observed. So it is possible to prepare test samples of the coatings without substrates with a thickness of 150–170 μm. By this procedure it was possible to measure the mechanical and thermal-mechanical properties of the coatings.

## 6. Mechanical and thermal-mechanical properties of BCN coatings

The prepared samples were tested in a bending test device at ambient temperature as a function of their density (Fig. 4). The greatest value of bending strength with 55 MPa was achieved by dense samples (density 99% TD). When the density of the samples decreases (97, 95, 93% TD), the bending strength decreases also (44, 37, 28 MPa, respectively).

It was not possible to determine the hot bending strength because we were not able to prepare the necessary sample geometry by plasma spraying.

Young modulus and modulus of rigidity were determined from 160–190 GPa and 38–46 GPa, respectively while Poison's ratio was about 0.33–0.35.

The hardness by Vickers was measured and resulted in values in the range of 3–5 GPa, dependant on the density of the coating and the thermal expansion coefficient was

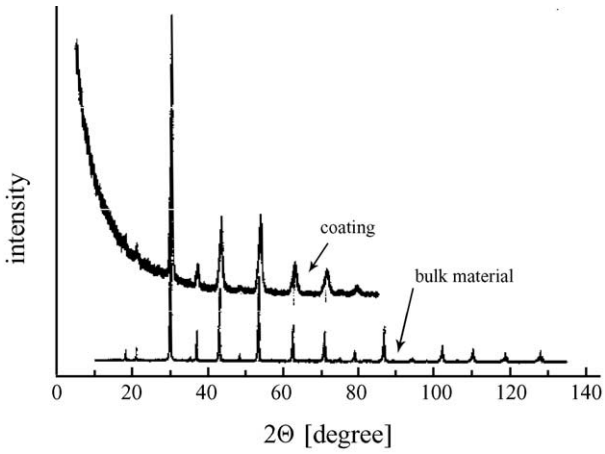


Fig. 3. X-ray diffraction pattern of BCN coating and bulk material.

in the range of $11.8\times10^{-6}$ $K^{-1}$ between ambient temperature and 1000 °C.

The thermal–mechanical properties of the coatings were tested by determination of the resistance to thermal shock with air quenching method for refractory bricks.[11] Thereby samples of 10 mm diameter and 10 mm height (coating on porous alumina substrate) were heated in an electric furnace till 800 °C and a stopping time of 15 min. Afterwards the samples were taken outside the furnace and air quenched (nozzle diameter: 5 mm; air pressure: 1 bar; distance between nozzle and sample: 100 mm) till 15 s. The number of nondestructive cycles is a criterion for the thermal shock resistance of the samples. If the sample resists 20 cycles the test will be break off. In the case of BCN 18 coatings 20 nondestructive cycles were reached.

The results were summarised in Table 4.

## 7. Preparation of thermal sprayed cermet coatings

First we had to determine the spraying parameters by variation of several parameters as described under Point 5 for the preparation of BCN coatings. The results of the investigation are listed in Table 5. The rich marked values represented the optimum spraying parameters in regard to coatings with high porosity. For the anode material, as well as for the cathode, a porosity of about 30% is necessary. The coating values we achieved were in the range of 86–81%, that means, porosity values of nearly 20% in maximum (Fig. 5).

Therefore we also tried to prepare cermet coatings by flame spraying technique to achieve coatings with the demand porosity. The flame spray device (Castolin, CastoDyn DS 8000) consists mainly of the burning gas containers (acetylene and oxygen), the flame spray gun and the powder feeder unit. Because of the cermet powder BCN 18/Ni the composition of the flame gases is so, that the nickel component do not

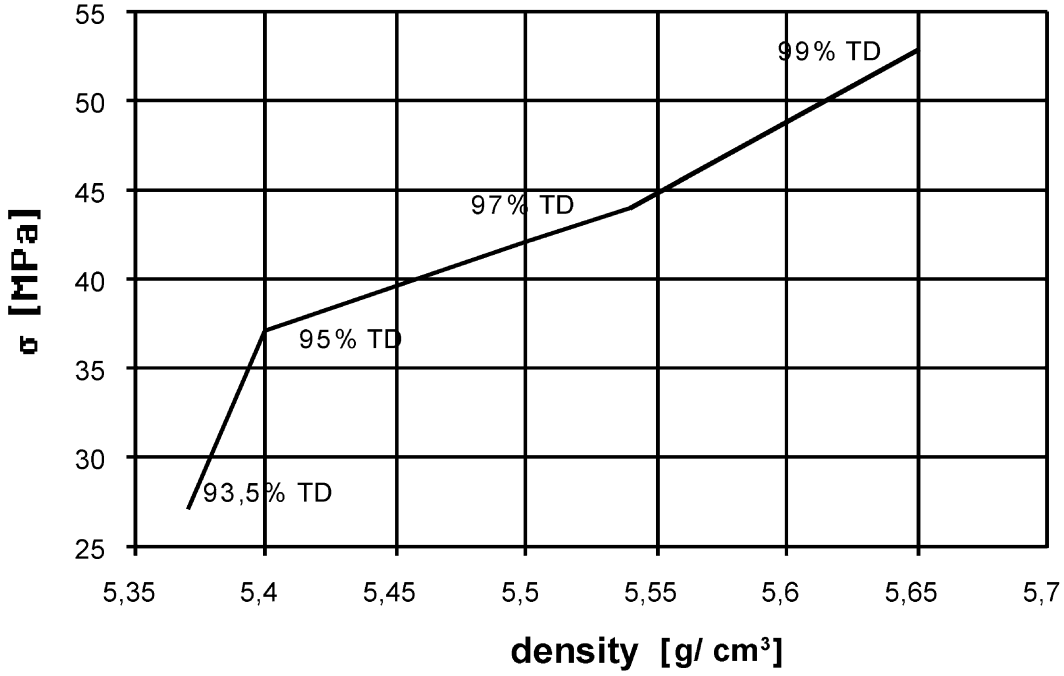


Fig. 4. Bending strength of BCN coatings as a function of density.

Table 4
Physical properties of BCN coatings

| | BCN Coating |
|---|---|
| Density | 99% TD[a] |
| Ultimate bending strength [MPa] | 50–55 |
| Bending strength (800 °C) [MPa | 5 |
| Hardness HV 1/10 [GPa] | 25 |
| Modulus of elasticity [GPa] | 190 |
| Modulus of rigidity [GPa] | 46 |
| Poisson's ratio $\mu$ | 0.35 |
| Thermal shock resistance | 20 cycles |
| Thermal expansion coefficient $\alpha$ $K^{-1}$ | 11.8 |

[a] Value of the theoritical density.

Table 5
Optimisation of the plasma spraying parameters for cermet coatings

| Primary gas $N_2$ [l/min] | Secondary gas 95/5 $N_2H_2$ [l/min] | Feeder gas $N_2$ [l/min] | Power [kW] | Spraying distance [cm] | Spraying time [min] |
|---|---|---|---|---|---|
| constant | **10** | 50 | 20 | 15 | 5 |
| **100** | 15 | **60** | 30 | **20** | **10** |
| | 20 | 80 | **40** | 30 | 20 |

Substrate: alumina membrane.

oxidised during the spraying process. The achieved cermet coatings were in the range of 75–70% TD. The substrate for the cermet coatings was stainless steel because of the bad adhesion of the coatings on this substrate. So we only got coatings for measuring their physical properties.

## 8. Mechanical and thermal-mechanical properties of cermet coatings

The prepared coating samples were also tested in a bending device at ambient temperature. The achieved bending strength was in the range of 39–54 MPa (30% porosity of the samples). The hot bending strength could not be measured, because it was not able to prepare an inert atmosphere inside the hot bending device. Otherwise the nickel particles of the cermet coatings were oxidised.

By the same way it was not possible to determine the thermal shock resistance of the cermet coatings. After two cycles all nickel particles were oxidised.

The Young's modulus was measured from 11 to 15 GPa while hardness was in the order of 0.2 GPa and the coefficient of thermal expansion about $11\times10^{-6}$ $K^{-1}$. The results were summarised in Table 6.

## 9. Preparation of ULSM–BCN and ULSM–BCN–BCN/Ni test samples

The ULSM powder was uniaxial cold pressed in steel moulds to green bodies of $10\times10\times50$ $mm^3$ and sintered at temperature of 1400 °C for 1 h. Afterwards the surface of the sintered parts were coated by plasma spraying of the BCN electrolyte. In the case of stacks the BCN electrolyte surface was coated by flame spraying of the BCN/Ni anode too. Than the pieces were sawn in samples of $40\times4\times3$ $mm^3$ and polished for the four-point bending tests.

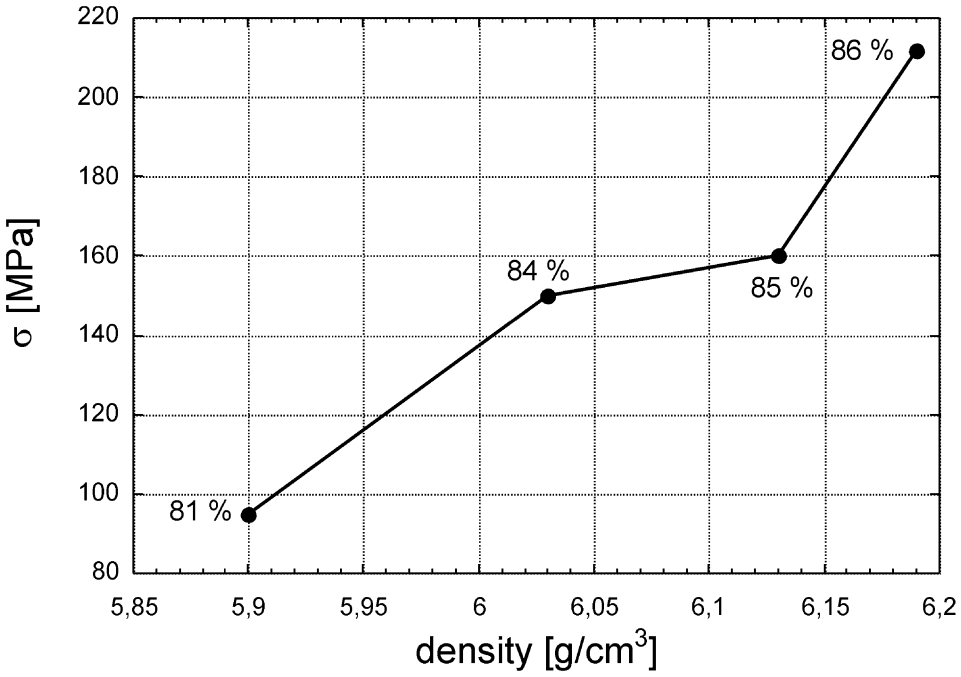


Fig. 5. Bending strength of cermet coating as a function of density.

Table 6
Physical properties of cermet coatings

| | BCN/Ni coating |
|---|---|
| Density | 70% TD[a] |
| Ultimate bending strength [MPa] | 54 |
| Modulus of elasticity [GPa] | 15 |
| Hardness HV 1/10 [GPa] | 0.2 |
| Thermal expansion coefficient $\alpha$ [$K^{-1}$] | 11 |

[a] Value of the theoritical density.

Table 7
Physical properties of material combination

| | Density [g/cm$^3$] | *E*-Modulus [GPa] | Bending strength [MPa] | Adhesion strength [MPa] |
|---|---|---|---|---|
| RT | 4.78 | 62 | 35.7 | 0.24 |
| 800 °C | / | 51 | 59 | / |

## 10. Mechanical and thermal–mechanical properties of ULSM–BCN material combination

The mechanical properties were examined due to bending strength at room temperature and higher temperature, Young's modulus (*E*) and adhesion strength.

The results of the four-point bending test at room temperature for the ULSM–BCN material was concluded in the following Table 7. The greatest value of 35 MPa maximum bending strength was achieved only by samples with a very good preparation.

The four-point bending test were performed at temperature of 800 °C and resulted in values of 59 MPa in maximum and *E* modulus of 51 GPa.

The adhesion strength was determined in variation of DIN 50 160: Testing of thermal sprayed metallic coatings; determination of adhesive strength in tension.[12] In Fig. 6 a scheme of the test is shown. Thereby the upper side of the cylindrically test samples (16 mm ø) were cemented on the cylindrically end of a steel rod (16 mm ø, 50 mm length) while the under side of the test samples

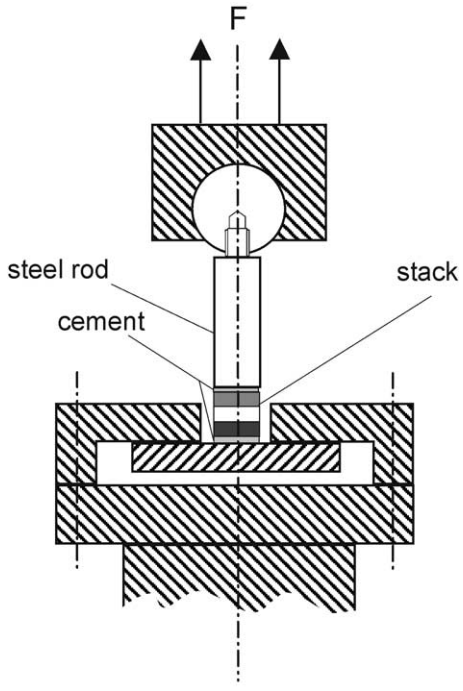


Fig. 6. Scheme of the test to determine adhesive strength.

were fixed on a steel plate $50\times50\times3$ mm$^3$) with a high-strength two-pack adhesive ($\sigma_z = 30$ MPa). In order to ensure accurate positioning, a special-purpose fixture was built, in which two specimens could be mounted for simultaneous cementing at exactly the right angle to minimise the occurrence of supplementary bending forces in the subsequent tensile test. The device (Fig. 6) with the specimens was fixed in a universal testing machine and loaded with a tensile force until fracture occur. The adhesion strength was calculated as a quotient of the measured force and the plane of the specimens. The values of the adhesive strength were in the range of 0.42 MPa (Table 7). In Fig. 7 a specimen after adhesive strength test is to be seen. In all cases the fracture mainly occur in the ULSM substrate.

## 11. Mechanical and thermal–mechanical properties of the stacks

First the adhesion strength of the prepared stacks were measured by determination of adhesive strength in tension test in variation of DIN 50 160[12] as we have done in the case of testing material combination ULSM–BCN. The results are listed in Table 8. The measured adhesive strength values were in the range of 0.42 MPa while the fracture of the stacks always occur in the ULSM substrate too. Otherwise the values were 75% higher than those of the material combinations.

The prepared stacks were also tested of their thermal shock resistance[3] as described in Point 6 by the properties of BCN coatings. The geometry of the samples was 16 mm ø and 10 mm high. In the case of stacks 20 nondestructive cycles were reached (Table 8).

## 12. Microscopic investigations

The microstructure of the sintered bodies and coatings was prepared by traditional ceramographic methods (sawing, grinding and polishing with diamond tools) and the grinding tests were investigated by scanning electron microscopy (SEM).

The figures show micro pictures of the tested SOFC compounds. In Fig. 8 the fracture surface of a ULSM sample is seen. The micro picture shows a very dense structure without pores. The shell shaped like morphology also indicates that the sample structure is very dense so that the fracture occurs transgranules, that means, through the grains. The grain size is in the range of 1–10 μm. On the other hand Fig. 9 shows the micro picture of a 30% porous ULSM samples. Thereby the porous structure can be seen very well.

Table 8
Physical properties of the stacks

| Density [g/cm$^3$] | Thermal shock resistance (Cycles) | Adhesion strength [MPa] |
|---|---|---|
| 4.77 | 15 to >20 | 0.42 |

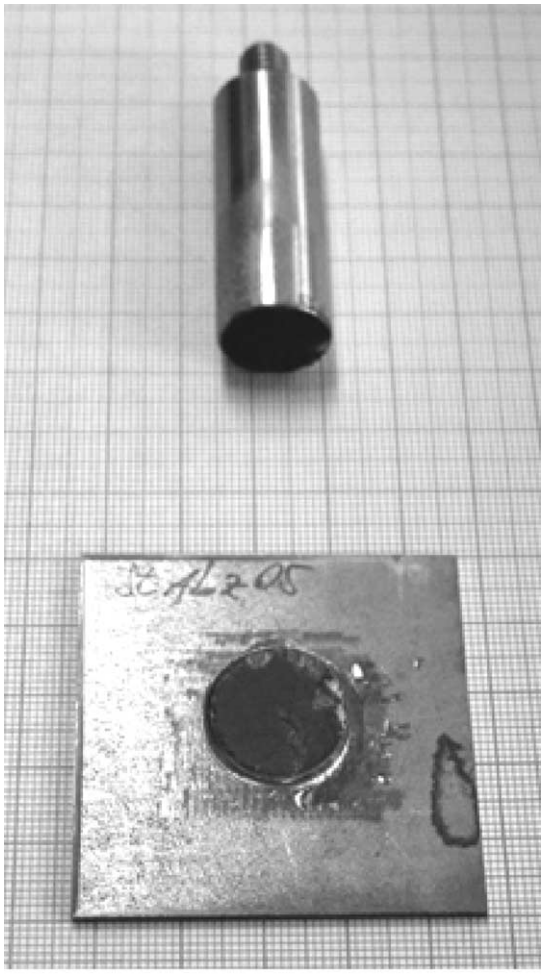

Fig. 7. Macro picture of prepared samples after adhesive strength test.

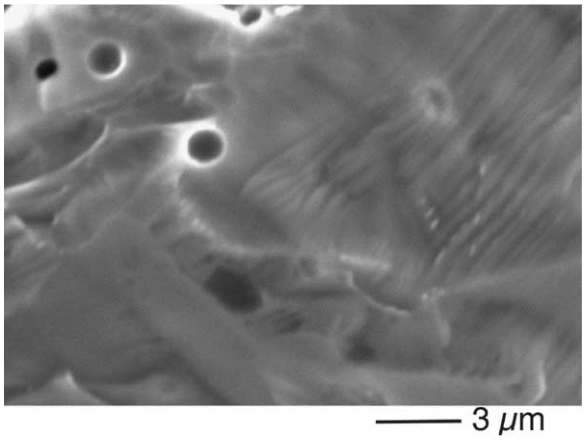


Fig. 8. SEM picture of a dense sintered ULSM sample.

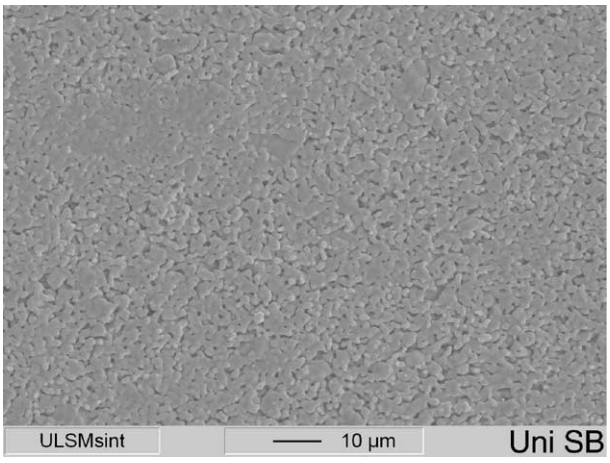


Fig. 9. SEM picture of a porous sintered ULSM sample.

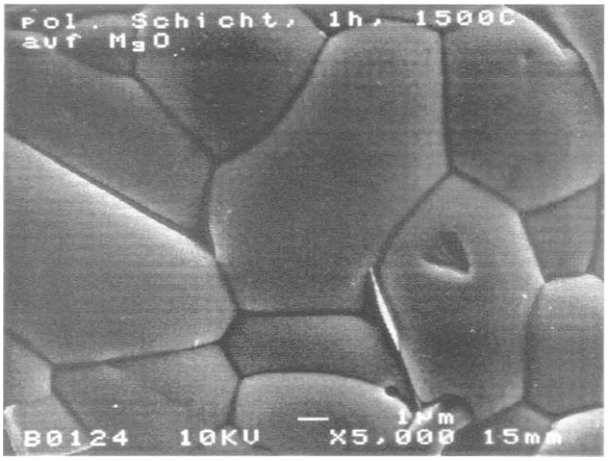


Fig. 11. HSEM picture of a sprayed and thermal etched BCN18 coating.

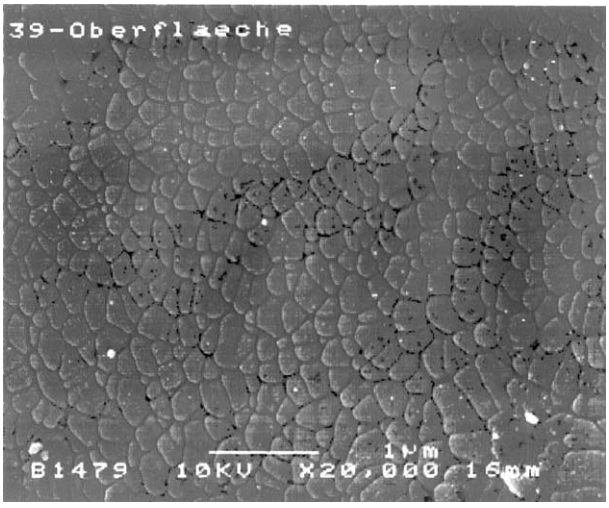


Fig. 10. HSEM picture of a BCN18 coating (surface).

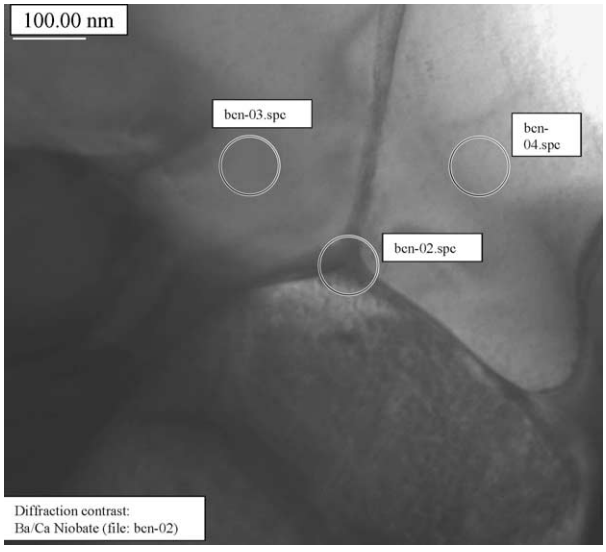


Fig. 12. TEM picture of a sprayed and thermal etched BCN18 coating.

The dense structure of a BCN18 coating surface can be seen in Fig. 10 prepared by high resolution scanning electron microscopy (HRSEM). The picture shows a very dense structure without any pores. All powder particles are melted by plasma spraying technique. The grain size is in the range of 0.09–0.5 µm. In the case of conductivity the grains are very fine so that the amount of grain boundary is to much and in consequence the conductivity very low. For increasing conductivity it is necessary to reduce the amount of grain boundary. Therefore we increase the grain size by thermal etching at 1500 °C for one hour. The result shows Fig. 11 where the enormous grain growth can be observed. The HSEM picture shows a BCN 18 coating surface polished and thermal etched so that the grain size is in the range of 3–12 µm. Finally the thermal etched coating samples were investigated by transmission electron microscopy (TEM). The prepared TEM picture can be seen in Fig. 12 where mainly three grains with their boundaries are shown. The three circles indicate the locations where EDX analysis has been done. The results are summarised in Fig. 13. The red curve indicates the amount of elements inside the grains while the blue curve indicates the amount of elements on the grain boundary. We can see that in the case of niobium a concentration on the grain boundary will be observed.

The cermet electrode was also investigated by SEM. The micro picture of the plasma sprayed BCN/Ni coating shows Fig. 14. The microstructure of the cermet is porous with a porosity of 20% in maximum depending on the various plasma spraying parameters. This amount of porosity is to small for the SOFC anode, so we tried to prepare the BCN/Ni anode by flame spraying technique. Hereby the sprayed particles were not accelerated so high in comparison to plasma spraying technique. Because of its lower flame temperature only the metallic Ni particles were melted.

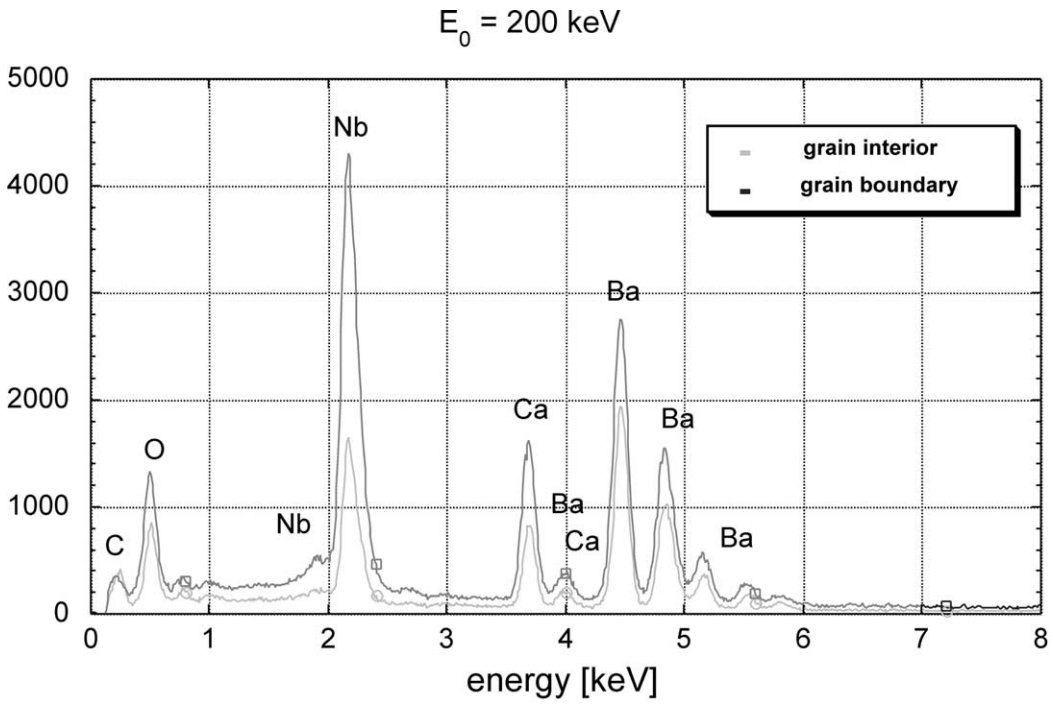


Fig. 13. TEM/EDXS diagram of Fig. 10.

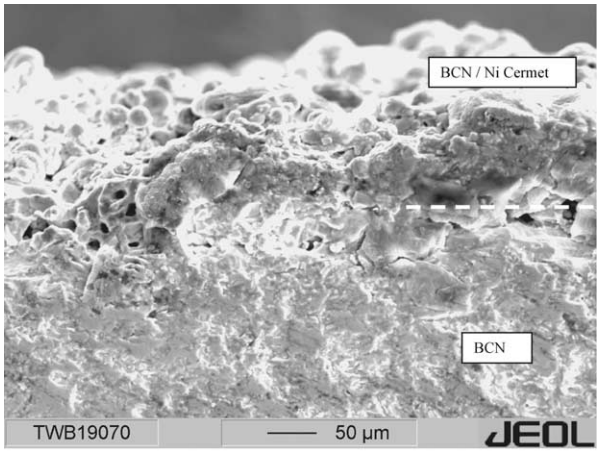


Fig. 14. SEM picture of a plasma sprayed cermet coating.

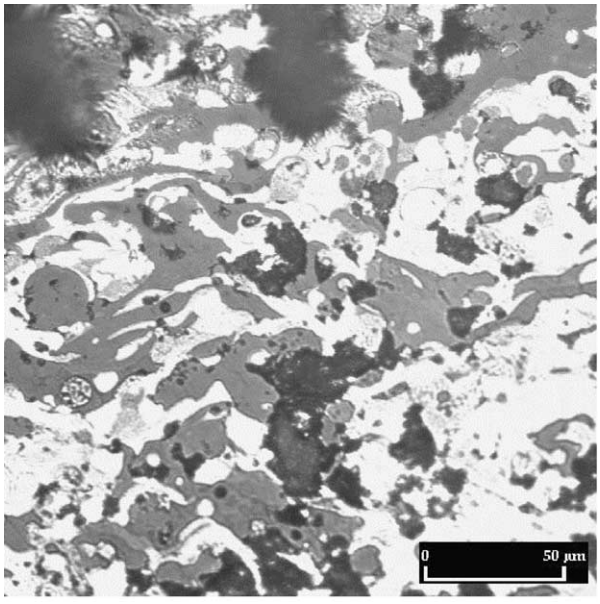


Fig. 15. Light-microscopy picture of a flame sprayed cermet coating.

The microstructure of the flame sprayed BCN/NI cermet coating can be seen in Fig. 15. With this spraying technique it was possible to reach the necessary porosity of 30% as to be seen in the micro picture.

The following figures show micro pictures of the tested SOFC material combination and the stacks. Fig. 16 shows the fracture surface of the material combination ULSM–BCN. In the picture no difference between the two materials can be recognised. That means the adhesion of the two materials may be good. No cracks are to be seen at the interfacial area. Fig. 17 represents the fracture surface of the material combination BCN–BCN/Ni. The different structure of the two materials can be identify very well like the fine structure of the BCN and the coarse structure of the cermet BCN/Ni. No cracks at the interface of the material combination mean a good adhesion of the two materials. Finally, Fig. 18 demonstrates the fracture surface of a whole stack. In the partial view of the picture prepared by optical microscopy the distribution of the metallic nickel phase into the cermet is to be seen.

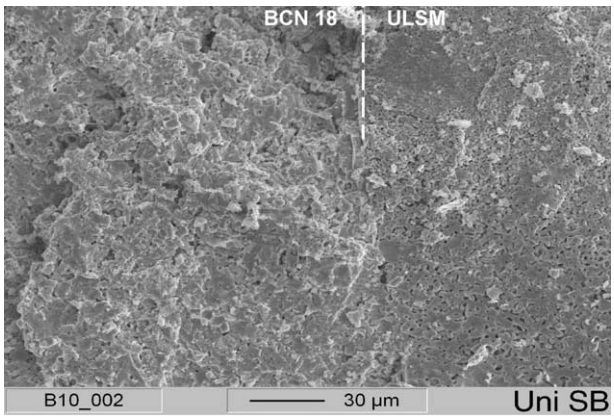


Fig. 16. SEM picture (fracture surface) of the material combination ULSM–BCN.

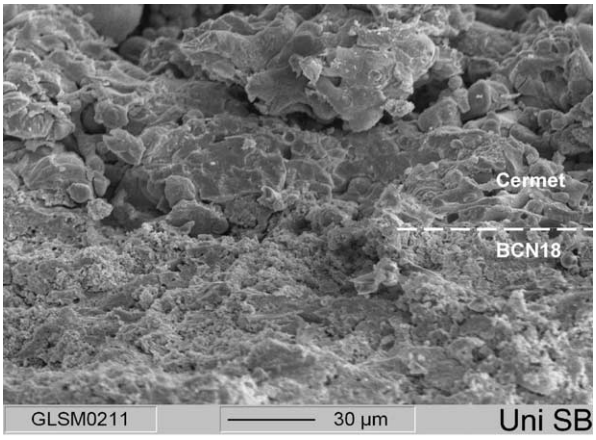


Fig. 17. SEM picture (fracture surface) of the material combination BCN–BCN/Ni.

## 13. Conclusion

All the examined materials for the electrodes or the electrolyte in a high temperature proton conducting solid oxide fuel cell (SOFC) seem to be potential candidate for a later use in the SOFC.

The ULSM-powder was synthesised by the carbonate route and solid state reaction. In this case the final product was achieved with a good output. The greatest value of cold bending strength of the sintered ULSM samples was achieved by the dense material. These correlated with the density and porosity, respectively. The necessary 30% porosity of the samples reached to a bending strength value high enough for a good handling of the samples. The hot bending strength (800 °C) was in the same order as the cold bending strength value.

In comparison to the BCN bulk material[1] the bending strength of the dense plasma sprayed BCN coatings was only half in values. The measurement of thin coatings in the bending test is very difficult and the strength is also a function of coating thickness. All other properties of the coatings are in the same order as the bulk material. It was not possible to measure the hot bending strength because the preparation of the necessary geometry of the test samples by plasma spraying was severe and not possible. For the hot bending device only the special geometry of the samples can be tested.

In the case of cermet coatings bending strength was a little bit lower than the strength of the BCN coatings. This can be explained by the high porous cermet coatings (30%). Also the hot bending strength could not be measured because, first, the necessary geometry of the samples could not prepared and, second, it was not possible to prepare an inert atmosphere inside the hot bending device.

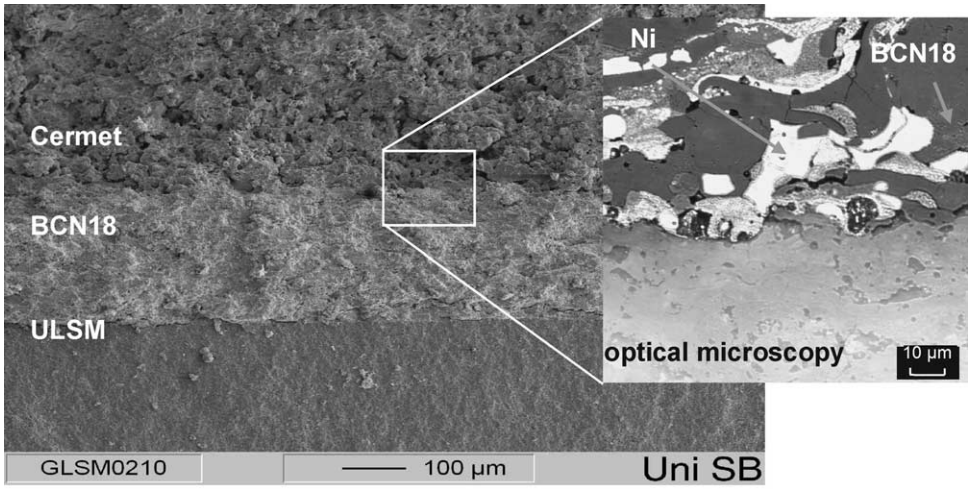


Fig. 18. SEM picture of a stack.

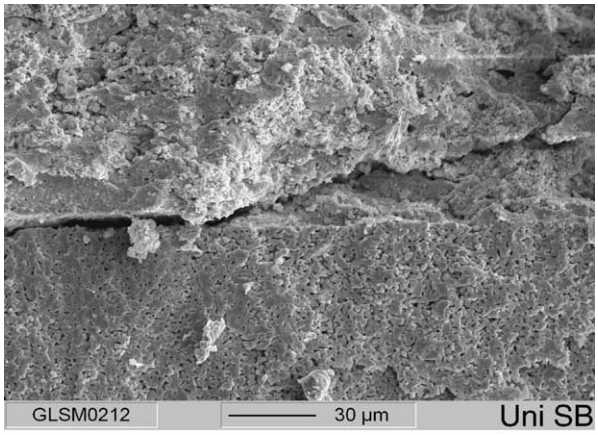


Fig. 19. SEM picture of a stack after thermal shock test.

The measurement of the expansion coefficient showed that the values are all at the same range between 11 and $12.8\times10^{-6}$ $K^{-1}$ and so a system can be built with these materials with a small quantity of strain.

The porous sintered ULSM samples were coated with BCN by plasma spraying. The measured cold bending strength of the material combination was in the order of 35 MPa and a little bit higher in values as the ULSM material only (26 MPa). Also hot bending strength shows the same tendency. The values of hot bending strength (800 °C) of the material combination were in the range of 59 MPa while ULSM alone reached values only at 25 MPa. This effect was also measured with BCN bulk material.[1]

The adhesive strength of the material combination was determined to 0.24 MPa while the fracture occurs always into the ULSM material. That means we do not measure the adhesive strength of the two materials but the tensile strength of the ULSM material as the weakest component.

On the other side, the resulted values of adhesive strength of the stacks were in the range of 0.42 MPa. The fracture occurs into the ULSM material too. Subsequently, we believe that the tensile strength of the ULSM material is in a wide range considering of the difficulties to determine tensile strength of ceramic materials.

The thermal shock resistance of the stacks was greater than 20 cycles, because if a sample resists 20 cycles the test will be break off. When samples resist 15 cycles only we saw that there were cracks along the interfacial area between ULSM and BCN as shown in Fig. 19.

## Acknowledgements

We wish to acknowledge and to thank the Deutsche Forschungsgemeinschaft (DFG) for the financial support of these investigations, which were performed in the Schwerpunktprogramm "Multifunktionswerkstoffe". We also thank Dr. T Krajewski, Institute of New Materials (INM), Saarbrücken, Germany for the TEM and TEM/EDXS investigations.

## References

1. Hassan, D., Janes, S. and Clasen, R., Proton-conducting ceramics as electrode/electrolyte materials for SOFC's, Part I: preparation, mechanical and thermal properties of sintered bodies. *J. Eur. Ceram. Soc.*, 2003, **23**, 221–228.
2. Weber, A., Waser, R. and Ivers-Tiffée, E., *Wechselwirkung zwischen Gefüge- und elektrischen Eigenschaften von Kathoden für die Festelektrolyt-Brennstofzelle* (SOFC). DKG-Jahrestagung, Kurzreferate, 1995, pp. 142–144.
3. Weber, A., Männer, R., Jobst, B., Schiele, M., Cerva, H., Waser, R. and Ivers-Tiffée, E., The influence of A-site-deficiency to the reaction kinetics of Sr doped La-Manganite perovskite type SOFC-cathodes. In *High Temperature Electrochemistry: Ceramics and Metals*, ed. F. W. Poulsen. Risoe National Laboratory, 1996.
4. De Souza, R., Islam, S. and Ivers-Tiffée, E., Formation and migration of cation defects in the perovskite oxide $LaMnO_3$. *J. Mat. Chemistry*, 1999, **9**, 1621–1628.
5. Herbstritt, D., Guntow, U., Weber, A., Müller, G. and Ivers-Tiffée, E., Increased cathode performance using a thin film LSM layer on a structured 8YSZ electrolyte surface. In *Proc. 10th Int. Conference on High Temperature Materials Chemistry*, 10–14 April, Jülich, Germany, 2000.
6. Herstritt, D., Weber, A., Müller, A., Guntow, U. and Ivers-Tiffée, E., Cathode performance: influence of MOD-intermediate layer and electrolyte surface enlargement. In *Proc. 4th European Solid Oxide Fuel Cell Conference*, ed. A. McEvoy. 10–14 July, Lucern, Swiss, 2000, The European Fuel Cell Forum, 2000, pp. 697–706.
7. Horita, T., Yamaji, K., Sakai, N., Yokokama, H., Weber, A. and Ivers-Tiffée, E., Stability at La0.6Sr0.4CoO3-d Cathode/La0.8Sr0.2Ga0.8Mg0.2O2.8 electrolyte interface under current flow for solid oxide fuel cell. *Solid State Ionics*, 2000, **138**, 143–152.
8. Müller, A., Pei, B., Weber, A. and Ivers-Tiffée, E., Properties of Ni/YSZ Cermets depending on their Microstructure. In *Proc. 10th Int. Conference on High Temperature Materials Chemistry,* 10–14 April, Jülich, Germany, 2000.
9. Müller, A., Herbstritt, D., Weber, A. and Ivers-Tiffée, E, Properties of Ni/8YSZ cermets for SOFC anodes: first steps in development of a multilayer anode. In *Proc. 4th European SOFC Forum*, ed. A. MaEvoy. Lucern, Swiss, The European Fuel Cell Forum, 2000, pp. 579–588.
10. Ivers-Tiffée, E., Weber, A. and Herbstritt, D., Materials and technologies for SOFC-components. *J. Eur. Ceram. Soc.*, 2001, **21**, 1805–1811.
11. DIN 51 068, Teil 2, Bestimmung des Widerstandes gegen schroffen Tempe-raturwechsel; Luftabschreckverfahren für feuerfeste Steine, 1980.
12. DIN 50 160, Ermittlung der Haft-Zugfestigkeit im Stirnzugversuch, 1977.